Escaping and transport barrier due to ergodic magnetic limiters in tokamaks with reversed magnetic shear

Elton C. da Silva[1]**, Marisa Roberto**[2]**, Jefferson S.E. Portela**[1]**, Iberê L. Caldas**[1] **and Ricardo L. Viana**[3]

[1] Instituto de Física, Universidade de São Paulo, C.P. 66318, 05315-970, São Paulo, São Paulo, Brazil
[2] Instituto Tecnológico de Aeronáutica, Centro Técnico Aeroespacial, Departamento de Física, 12228-900, São José dos Campos, São Paulo, Brazil
[3] Departamento de Física, Universidade Federal do Paraná, C.P . 19081, 81531-990, Curitiba, Paraná, Brazil

E-mail: ibere@if.usp.br

Abstract
Analytical tokamak plasma equilibria, with non-monotonic plasma current profile and perturbed by ergodic magnetic limiters, are described by non-twist conservative maps. Examples are given of concentration of magnetic field lines escaping to the tokamak wall. The robustness of invariant curves on the shearless region is also observed.

PACS numbers: 05.45.Ac, 05.45.Pq, 52.25.Fi

1. Introduction

The presence of non-integrable magnetic field lines in a certain plasma region within the tokamak implies the loss of the plasma confinement, due to the absence of flux surfaces. However, the chaotization of a limited plasma region, if properly handled, can be beneficial to the plasma confinement, as exemplified by the ergodic magnetic limiter [1–5] and the Dynamic Ergodic Divertor at TEXTOR tokamak [6]. Another situation in which the presence of non-integrable magnetic fields can help plasma confinement is the creation of a barrier to reduce Lagrangian field line escape in tokamaks with a negative magnetic shear region. Such a region is created by means of a non-peaked plasma current density, corresponding to a non-monotonic radial profile for the safety factor [7]. A resonant magnetic perturbation in the shearless region gives rise to a barrier separating the internal region with magnetic surfaces from the external stochastic region. The field line escape outside the barrier, at the plasma edge, is similar to those observed for monotonic equilibria. In fact, outside the barrier, the safety factor increases monotonically. The presence of the Lagrangian barrier in the shearless region limits the volume of the escape region. All this may contribute to the enhanced plasma confinement which has been observed in some experiments with magnetic shearless equilibria [8, 9].

Unlike most magnetic configurations, negative shear configurations are best described by non-twist area-preserving maps [10, 11]. Such maps violate the non-degeneracy condition for the Kolmogorov–Arnold–Moser (KAM) theorem to be valid, so that many well-known results of canonical mappings no longer apply to them [12–14]. For example, it may happen that two neighbour island chains approach each other without being destroyed through the breakup of KAM curves [15]. The transport barrier arises from a combination of typical features of non-twist maps: reconnection and bifurcation, occurring in the reversed shear region [16]. This barrier is embedded in a chaotic field line region located in the tokamak peripheral region. Further investigation of this barrier requires a conservative map like the ones used in this article.

In this paper we introduce non-twist maps obtained by considering the superposition of an ergodic magnetic limiter field on the tokamak equilibrium field with a negative shear region due to a non-peaked plasma current. The limiter perturbation generates resonant magnetic fields that interact with the equilibrium field, causing a selective destruction of the magnetic surfaces at the plasma edge. On the inner plasma region, the field lines lie on magnetic surfaces, while the chaotic and unstable periodic lines are in the outer scrape-off layer. The external chaotic layer configuration is essentially

determined by the chaotic set on the scrape-off layer [17–21]. As a consequence of this chaotic configuration, the field lines with long connection lengths hit the tokamak wall non-uniformly producing the so-called field line escape pattern.

In this work, we use one of the introduced non-twist maps to study the connection of the chaotic lines to the tokamak wall. These maps are also used to numerically evidence the formation of a transport barrier due to a reconnection–bifurcation mechanism, and its effect on the plasma transport can be inferred from the study of field line diffusion by using the obtained maps.

The paper is organized as follows: in section 2, we present an area-preserving non-twist map to study, in toroidal geometry, the field line escaping to the tokamak wall. In section 3, we introduce another symplectic non-twist map to study the robustness of the internal shearless barriers in large aspect ratio tokamaks. Our conclusions are presented in the last section.

2. Field line escaping

In this section, we study the Lagrangian field line transport and the line escaping to the tokamak wall for a plasma equilibrium with reversed magnetic shear. We use a suitable coordinate system to describe magnetic field line geometry in a tokamak: $(r_t, \theta_t, \varphi_t)$, given by [22]

$$r_t = \frac{R_0'}{\cosh(\xi) - \cos(\omega)}, \tag{1}$$

$$\theta_t = \pi - \omega, \tag{2}$$

$$\varphi_t = \Phi, \tag{3}$$

in terms of the usual toroidal coordinates (ξ, ω, Φ) as presented in [23]. The meaning of these variables is the following: r_t is related to the radial coordinate of a field line with respect to the magnetic axis. R_0' is the major radius with respect to the magnetic axis. R_0 and b are (see figure 1(a)), respectively, the major and minor radii with respect to the geometric axis. The angles θ_t and φ_t are, respectively, the poloidal and toroidal angles of this field line.

The contravariant components of the tokamak equilibrium magnetic field $\boldsymbol{B}_0 = (0, B_0^{(2)}, B_0^{(3)})$ are obtained from an approximated analytical solution of the equilibrium magneto-hydro-dynamical equation in these coordinates [24]. Figure 2 shows the normalized equatorial profiles of the poloidal and toroidal contravariant components of $\boldsymbol{B}_0$, respectively, for the equilibrium with reversed magnetic shear considered in this work.

In order to generate the reversed shear region we have considered a toroidal current density profile

$$j_{\varphi_t}(r_t) = \frac{I_p R_0'}{\pi a^2} \frac{(\gamma + 2)(\gamma + 1)}{\beta + \gamma + 2} \left[1 + \beta \left(\frac{r_t}{a} \right)^2 \right] \left[1 - \left(\frac{r_t}{a} \right)^2 \right]^\gamma, \tag{4}$$

with a central hole [25, 16]. In equation (4), β and γ are parameters that can be chosen to fit experimentally observed plasma profiles. The result is that the safety factor of the magnetic surfaces, defined as [26]

$$q(r_t) = \frac{1}{2\pi} \int_0^{2\pi} \frac{B_0^{(3)}(r_t, \theta_t)}{B_0^{(2)}(r_t)} d\theta_t, \tag{5}$$
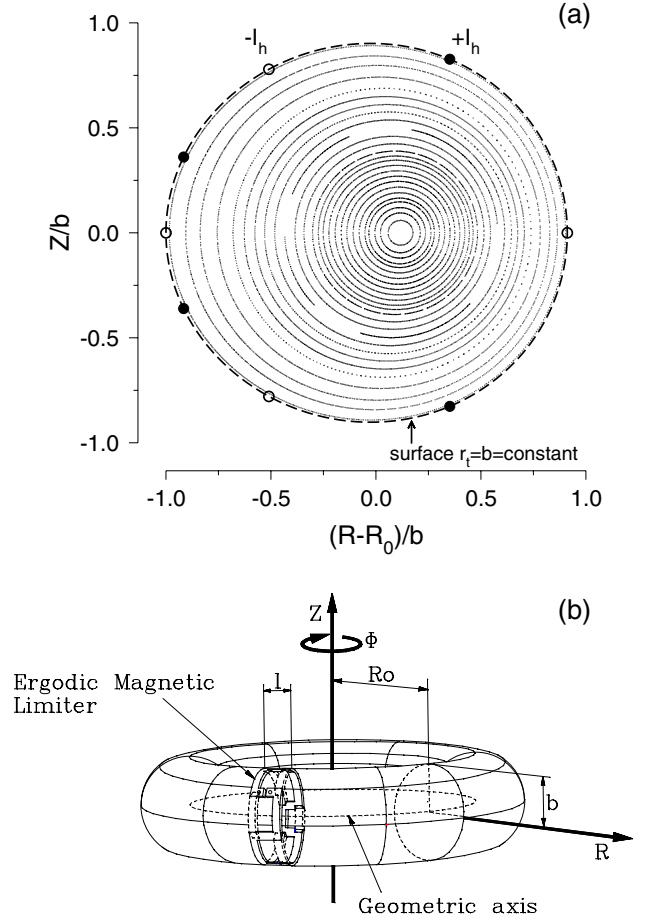

Figure 1. (a) Basic geometry of the tokamak; (b) scheme of an ergodic magnetic limiter.

has a non-monotonic profile. For $\beta \neq 0$ the safety factor has two different magnetic surfaces within the plasma column [25, 16] (see figure 3).

The ergodic magnetic limiter consists of N_r current rings of length ℓ located symmetrically along the toroidal direction of the tokamak (figure 1(b)). These current rings may be regarded as slices of a pair of external helical windings located at $r_t = b$, conducting a current I_h in opposite senses for adjacent conductors. The role of these windings is to induce a resonant perturbation in the tokamak, and to achieve this effect a tunable parameter, λ, is introduced such that the helical windings have the same pitch as the field lines in the rational surface we want to perturb. This has been carried out by choosing the following winding law [24] $u_t = m_0[\theta_t + \lambda \sin(\theta_t)] - n_0 \varphi_t = \text{constant}$, where (m_0, n_0) are the poloidal and toroidal mode numbers, respectively.

The magnetic field $\boldsymbol{B}_1$ produced by the resonant helical windings, from which we build the EML rings, is obtained by neglecting the plasma response and the penetration time through the tokamak wall. We are able to obtain an approximated analytical solution in lowest order for the limiter field, by solving the corresponding boundary value problem. The model field to be used in this paper is the superposition of the equilibrium and limiter fields: $\boldsymbol{B} = \boldsymbol{B}_0 + \boldsymbol{B}_1$. Since the equilibrium field is axisymmetric, we may set the azimuthal angle, $\varphi_t = t$, as a time-like variable and put the magnetic field
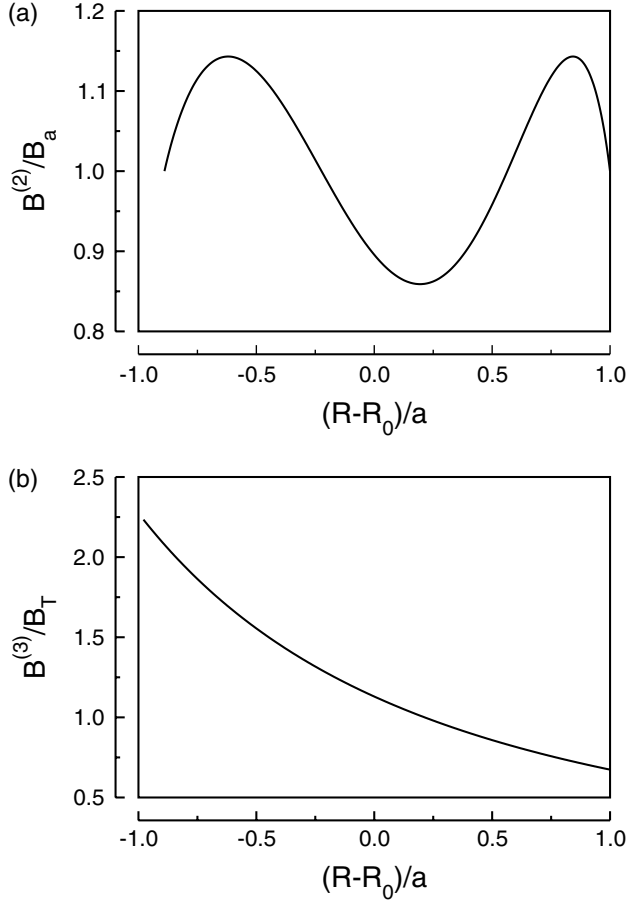
(a)

(b)

Figure 2. Profiles of the poloidal (*a*) and toroidal (*b*) contravariant components of the equilibrium magnetic field with reversed shear.
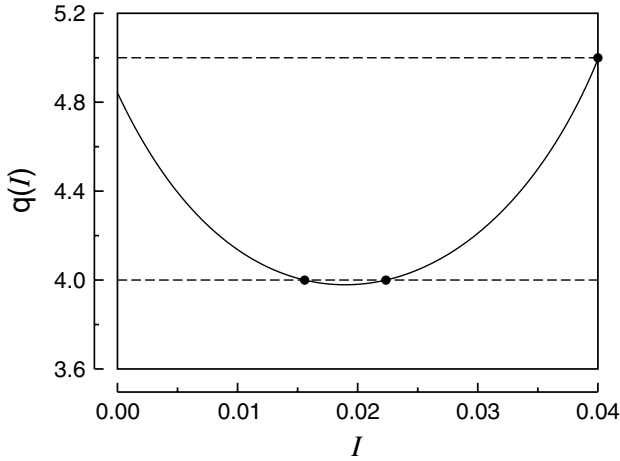

Figure 3. Profile of the safety factor for a reversed shear configuration of a tokamak in terms of the action variable.

line equations in a Hamiltonian form [27]

$$\frac{\mathrm{d}\mathcal{I}}{\mathrm{d}t} = -\frac{\partial H}{\partial \vartheta}, \tag{6}$$

$$\frac{\mathrm{d}\vartheta}{\mathrm{d}t} = \frac{\partial H}{\partial \mathcal{I}}, \tag{7}$$

where $(\mathcal{I}, \vartheta)$ are the action–angle variables of a Hamiltonian H, its explicit form being given by

$$\mathcal{I}(r_t) = \frac{1}{4}\left[1 - \Omega_+(r_t) \cdot \Omega_-(r_t)\right], \tag{8}$$

$$\vartheta(r_t, \theta_t) = 2\arctan\left[\frac{\Omega_+(r_t)}{\Omega_-(r_t)}\tan\left(\frac{\theta_t}{2}\right)\right], \tag{9}$$

where

$$\Omega_\pm(r_t) = \sqrt{1 \pm 2\frac{r_t}{R_0'}}. \tag{10}$$

The addition of the magnetic field produced by resonant helical windings may be regarded as a Hamiltonian perturbation. In order to include the effect of the finite length ℓ of each EML ring, which is typically a small fraction of the total toroidal circumference $2\pi R_0'$, we model its effect as a sequence of delta-functions centred at each ring position. The Hamiltonian for the system is thus

$$H(\mathcal{I}, \vartheta, t) = H_0(\mathcal{I}) + \epsilon H_1(\mathcal{I}, \vartheta, t)\sum_{k=-\infty}^{+\infty}\delta\left(t - k\frac{2\pi}{N_r}\right), \tag{11}$$

where

$$H_0(\mathcal{I}) = \int\frac{2\pi\,\mathrm{d}\mathcal{I}}{q(r_t(\mathcal{I}))} \quad \text{and} \quad H_1(\mathcal{I}, \vartheta, t) = \sum_{m=0}^{2m_0}H_m^*(\mathcal{I})e^{i(m\vartheta - n_0 t)}, \tag{12}$$

with

$$H_m^*(\mathcal{I}) = \sum_{m'=0}^{2m_0}H_{m'}(r_t(\mathcal{I})) \cdot S_{m,m'}(\mathcal{I}), \tag{13}$$

$$H_{m'}(r_t) = -J_{m'-m_0}(m_0\lambda)\left(\frac{r_t}{b}\right)^{m'}, \tag{14}$$

$$S_{m,m'}(\mathcal{I}) = \frac{1}{2\pi}\int_0^{2\pi}e^{i[m'\theta_t(\mathcal{I},\vartheta) - m\vartheta]}\mathrm{d}\vartheta. \tag{15}$$

Due to the t-dependence of the Hamiltonian in the form of a sequence of delta-functions, it is possible to define discretized variables $(\mathcal{I}_n, \vartheta_n)$ as the corresponding values of the angle–action variables just after the nth crossing of a field line with the plane $t_k = (2\pi k/N_r)$ with $k = 0, 1, 2, \ldots, N_r - 1$ [28]. Proceeding in this fashion, the following area-preserving mapping can be associated with the EML Hamiltonian (equation (11)) [24]:

$$\mathcal{I}_{n+1} = \mathcal{I}_n + \epsilon f(\mathcal{I}_{n+1}, \vartheta_n, t_n), \tag{16}$$

$$\vartheta_{n+1} = \vartheta_n + \frac{2\pi}{N_r q(\mathcal{I}_{n+1})} + \epsilon g(\mathcal{I}_{n+1}, \vartheta_n, t_n), \tag{17}$$

$$t_{n+1} = t_n + \frac{2\pi}{N_r}, \tag{18}$$

with

$$f = -\frac{\partial H_1}{\partial \vartheta}, \qquad g = \frac{\partial H_1}{\partial \mathcal{I}} \qquad \text{and} \qquad \epsilon = 2\frac{I_h l}{I_e R_0'}, \tag{19}$$

where l is the EML coil width and I_e is the total current on the solenoid that creates the toroidal magnetic field.

It should be remarked, however, that the integration along the delta functions is not well defined. A more exact
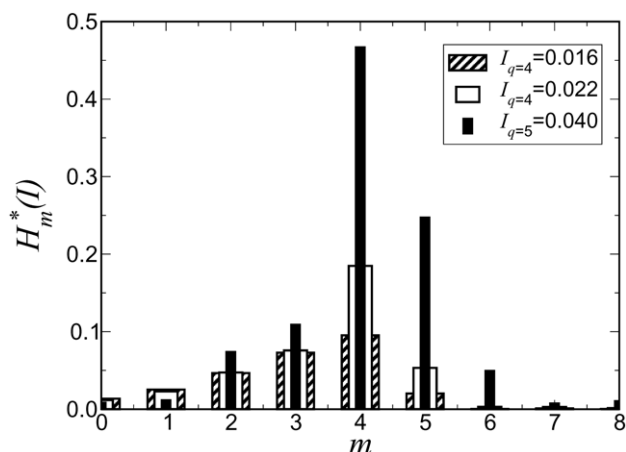
Figure 4. Poloidal distribution of the EML modes.

perturbative method of construction of symplectic maps for Hamiltonian systems of the type of equation (11) has been recently developed [29, 30]. According to this method, the exact mapping for the Hamiltonian given by equation (11) has a symmetric form, in the sense discussed in [31]. Our non-symmetric mapping equations (equations (16)–(19)) can be obtained as an approximation of the exact symmetric map only for small perturbations and a weak dependence of the perturbation Hamiltonian, $H_1(\mathcal{I}, \vartheta, t)$, on the toroidal flux.

The Hamiltonian treatment of field line flow is useful to study the creation of a chaotic magnetic field line layer in the plasma due to the interaction between resonant perturbing fields and the tokamak equilibrium magnetic field [33]. Here the word *chaos* must be intended in its Lagrangian sense: two field lines very close to each other, depart exponentially as we follow their revolutions along the toroidal chamber. In terms of the field line map, chaos means an area-filling orbit in the surface of section, through which a field line can wander erratically.

Figure 4 shows the Fourier poloidal distribution of the EML perturbation for $m_0 = 4$. The main modes created by the EML are $m = 4$ and $m = 5$.

The stochastic condition could be estimated from the overlapping condition of islands. The mode amplitudes (figure 4) and the q profile at their resonant surfaces determine this condition [32].

Figure 5 shows two Poincaré cross-sections produced by the area-preserving mapping, given by equations (16)–(18), for $I_h = 2\%$ of I_p, where I_p is the plasma current. We choose $\gamma = 0.75$ and $\beta = 2.80$ corresponding to the non-monotonic q profile of figure 3. The perturbing parameter $\lambda = 0.4327$ is used in order to focus the perturbation on the most external surface with $q = 4$. The maps show the islands due to the main resonances observed in the poloidal spectrum of figure 4. Figure 5(a) displays well-known features comprising (i) chains of islands which appear due to the breaking of equilibrium flux surfaces with rational q values; (ii) KAM tori formed by surviving, although deformed, flux surfaces for which q is irrational and (iii) chaotic area-filling field lines which appear due to the crossing of homoclinic/heteroclinic invariant manifolds of unstable periodic orbits. Increasing the perturbing current to $I_h = 8.3\%$ of I_p (figure 5(b)),
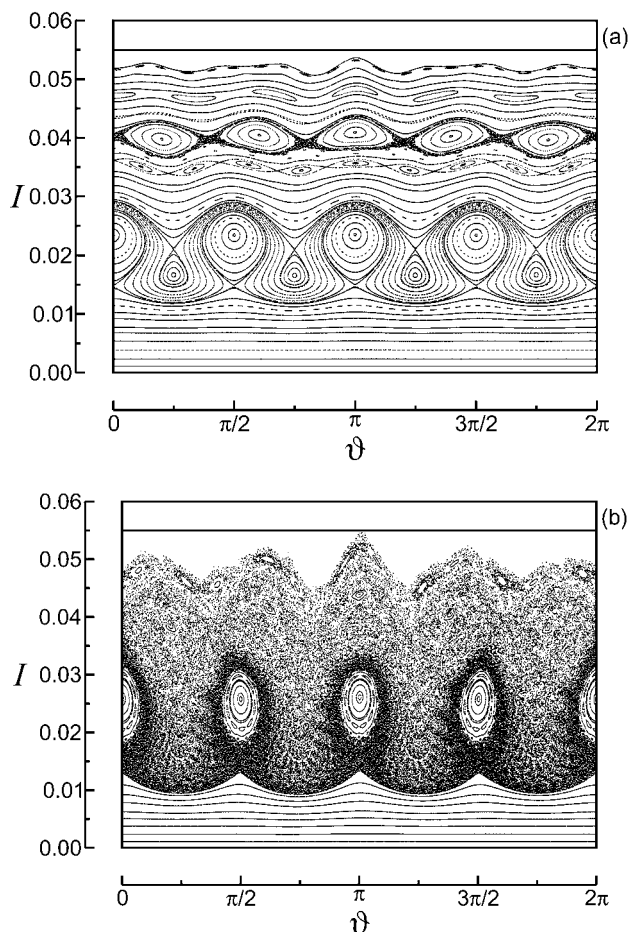

Figure 5. Poincaré cross-section, in terms of the angle–action variables, produced by the EML mapping. Non-monotonic q profile with $\gamma = 0.75$ and $\beta = 2.80$, $N_r = 4$, $(m_0, n_0) = (4, 1)$, $\lambda = 0.4327$. (a) $I_h = 2\%$ of I_p and (b) $I_h = 8.3\%$ of I_p.

the last barrier between the plasma and the tokamak wall is destructed and a wide region of chaotic field lines is produced. Surrounding the remaining $q = 4$ islands chain there is a sticking region where field lines stay for a long time before eventually escaping and reaching the wall. The observed field line trapping on the shearless region produces an effect similar to that of a transport barrier and is interpreted in terms of an invariant chaotic set around this region. Thus, the formation of the chaotic layer at the plasma edge is determined by the invariant sets, such as the stable and unstable manifolds and the chaotic saddles of unstable periodic lines that exist in this region. Moreover, we study the resonant perturbation field lines considering the so-called exit basins or sets of points in the chaotic region which originate field lines that hit the wall in some specified region. This investigation shows that, for a tokamak with reversed magnetic shear, depending on the perturbed magnetic configuration, the field line escape pattern spreads over the tokamak wall or concentrates on its external equatorial region [17]. In particular, in figure 5(b), we observe that the field lines, which eventually escape, reach the wall in a very thin region, around $\theta_t = \pi$, on the external equatorial plane.

Experimental evidence of the influence of chaotic scrape-off layers on the plasma confinement, with magnetic field line

shear, have been recently reported [18, 34]. This evidence confirms the importance of invariant chaotic saddles to predict the scrape-off layer magnetic structures [19–21].

3. Transport barrier

The basic geometry of a tokamak is determined by its major (R_0) and minor (b) radii (figure 1(a)). When the tokamak aspect ratio R_0/b is large enough we can neglect, in a zeroth approximation, the effects of the toroidal curvature and treat it as a periodic cylinder of length $2\pi R_0$, whose axis of symmetry is parametrized by the coordinate $z = R_0\varphi$ in terms of the toroidal angle φ [26]. In this case, the equilibrium toroidal field B_0 is practically uniform. Accordingly, a point in the tokamak is located by its cylindrical coordinates (r, θ, z) with respect to that axis. On the other hand, in the study of the region near the tokamak wall, it turns out that even the poloidal curvature does not change results noticeably, so that a rectangular system can be found by defining the following coordinates: $x' = b\theta$ and $y' = b - r$ [35]. The tokamak wall is thus characterized by the line segment $y' = 0$ extending from $x' = 0$ to $2\pi b$. In the following we will use normalized coordinates $x = x'/b$ and $y = y'/b$.

In the description used in this section the structure of the magnetic field lines in a tokamak can be more easily appreciated by taking a Poincaré surface of section at the plane $z = 0$. Let (r_n, θ_n) be the polar coordinates of the nth piercing of a given field line with that surface. Since the magnetic field line equations determine uniquely the position of the next piercing, we have a Poincaré map $(r_{n+1}, \theta_{n+1})^T = \boldsymbol{F}_1(r_n, \theta_n)^T$. Due to the solenoidal character of the magnetic field, this map is area-preserving in the surface of section [36]. The regular orbits lay in invariants magnetic surfaces described by the equation

$$\frac{r \, \mathrm{d}\varphi}{R_0 \, \mathrm{d}\theta} = q, \tag{20}$$

where θ and φ are the angles on the surface identified by the safety factor q.

In the absence of any perturbation, the configuration is described by a map $(r_n^*, \theta_n^*)^T = \boldsymbol{F}_1(r_n, \theta_n)^T$ [37], where

$$r_n^* = \frac{r_n}{1 - a_1 \sin\theta_n}, \tag{21}$$

$$\theta_n^* = \theta_n + \frac{2\pi}{q(r_n^*)} + a_1 \cos\theta_n, \tag{22}$$

which have a correction for the effect of the toroidal curvature whose strength is given by the a_1 parameter.

The dependence of the safety factor with the radius is dictated by the details of the equilibrium magnetic field. The following expression describes in a satisfactory way typical non-monotonic q profiles of plasma discharges in tokamak experiments [25]:

$$q(r) = q_a \frac{r^2}{a^2} \left[1 - \left(1 + \beta' \frac{r^2}{a^2} \right) \left(1 - \frac{r^2}{a^2} \right)^{\gamma+1} \Theta(a - r) \right]^{-1}, \tag{23}$$

where a is the plasma radius (slightly less then the tokamak minor radius b), q_a, β and γ are parameters that can be chosen to fit experimentally observed plasma profiles ($\beta' =$
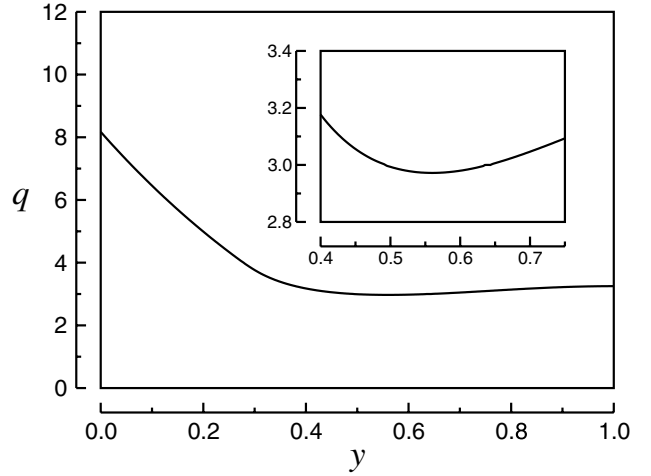

Figure 6. Safety factor profile.

$\beta(\gamma + 1)/(\beta + \gamma + 1))$ and $\Theta(\cdot)$ is the unit step function. We choose $\beta = 2$ and $\gamma = 1$ that results in a slightly non-monotonic profile with a minimum near $y = 0.5$ (figure 6).

We consider the ergodic magnetic limiter introduced in the previous section. The effect of the EML on the equilibrium configuration can be approximated by a sequence of delta function pulses at each piercing of a field line in the surface of section. In cylindrical approximation [3, 28, 35], such a mapping $(r_{n+1}, \theta_{n+1})^T = \boldsymbol{F}_2(r_n^*, \theta_n^*)^T$ has been described by [37]:

$$r_n^* = r_{n+1} + \frac{m_0 C b}{m_0 - 1} \left(\frac{r_{n+1}}{b} \right)^{m_0 - 1} \sin(m_0 \theta_n^*), \tag{24}$$

$$\theta_{n+1} = \theta_n^* - C \left(\frac{r_{n+1}}{b} \right)^{m_0 - 2} \cos(m_0 \theta_n^*), \tag{25}$$

where $C = (2m_0 l a^2 / R_0 q_a b^2)(I_h/I_p) \approx 1.6 \cdot 10^{-1} I_h/I_p$ represents the perturbation strength due to the magnetic ergodic limiter. In the following, we use the ratio between the limiter and plasma currents, I_h/I_p, to quantify the perturbation strength. In this section this ratio varies from 0.1 to 0.3 assuring a small value for the perturbation strength.

The entire field line mapping is the composition of the two mappings ($\boldsymbol{F} = \boldsymbol{F}_1 \circ \boldsymbol{F}_2$) and, since the variable r_{n+1} appears in both sides of the expression, we must solve for it at each iteration using a numerical scheme (Newton–Raphson method).

Symplectic mappings are convenient and fast ways of describing field line behaviour in tokamaks with ergodic limiters, since we do not need to numerically integrate the field line equations over the whole toroidal revolution, in order to get the coordinates of a field line intersection with the Poincaré surface of section. The mapping $\boldsymbol{F}$ is strictly area-preserving. However, as the variables (r, θ) are not canonical, this map preserves the magnetic flux only approximately.

The phase portraits of figure 7 show, for $m_0 = 3$, the scenario of separatrix reconnection [15]: due to the non-monotonicity [12] of our map, there are two island chains with the same period separated by invariant curves (a); increasing the perturbation the islands widen and the separatrices merge (b); then the chains interchange their hyperbolic points (c).
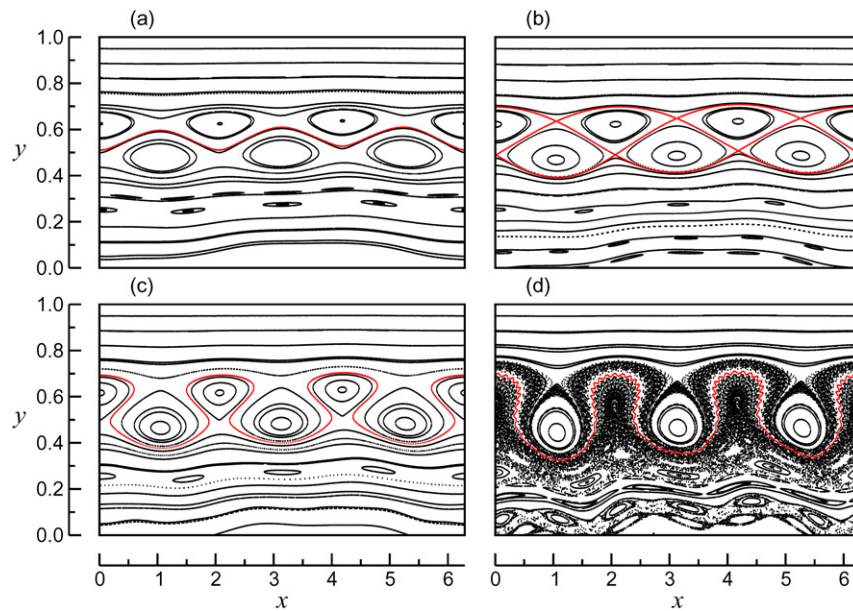
Figure 7. Phase portraits exhibiting the reconnection scenario: (*a*) $I_h/I_p = 0.05$, there are two island chains; (*b*) $I_h/I_p = 0.0635$, an heteroclinic connection takes place; (*c*) $I_h/I_p = 0.10$, the chains interchanged hyperbolic points; (*d*) $I_h/I_p = 0.30$, one of the island chains disappeared in a bifurcation and a barrier persists.

(This figure is in colour only in the electronic version)

Figure 7 also exhibits a bifurcation, the disappearance of an island chain due to the collision of its elliptic and hyperbolic points (*d*), as well as the rising and persistence of a transport barrier separating the chaotic region in the phase space.

The barrier turns out to be very robust, resisting perturbations up to $I_h/I_p = 0.30$. The barrier exists whenever we find an orbit describing an invariant curve. We establish a limit to the perturbation necessary to destroy the barrier as $I_h/I_p = 0.3030$ by verifying whether or not a long trajectory (we use 10^{11} iterations) passes through the barrier. Figure 8 shows the barrier breaking.

4. Conclusions

We use analytically obtained non-twist field line maps to study the effects of an ergodic magnetic limiter on the magnetic field line structure which results from a plasma current profile exhibiting reversed magnetic shear.

The non-twist nature of the maps allows island chains to approach and dimerize, as the limiter current builds up, in a reconnective process. The creation of a reasonably wide chaotic layer is predicted by global stochasticity mechanisms, eventually forming a chaotic region.

In the external part of the chaotic layer, the field lines escape to the wall and, depending on the equilibrium and perturbation parameters, their connections to the wall may concentrate on a small region. This concentrated connections should be disadvantageous for the plasma confinement. The same disadvantage may also be observed for equilibria with monotonic profiles [17].

Inside the plasma, a Lagrangian barrier may be created. This barrier is formed in the shearless plasma and results from the properties of field line trajectories in the vicinity of
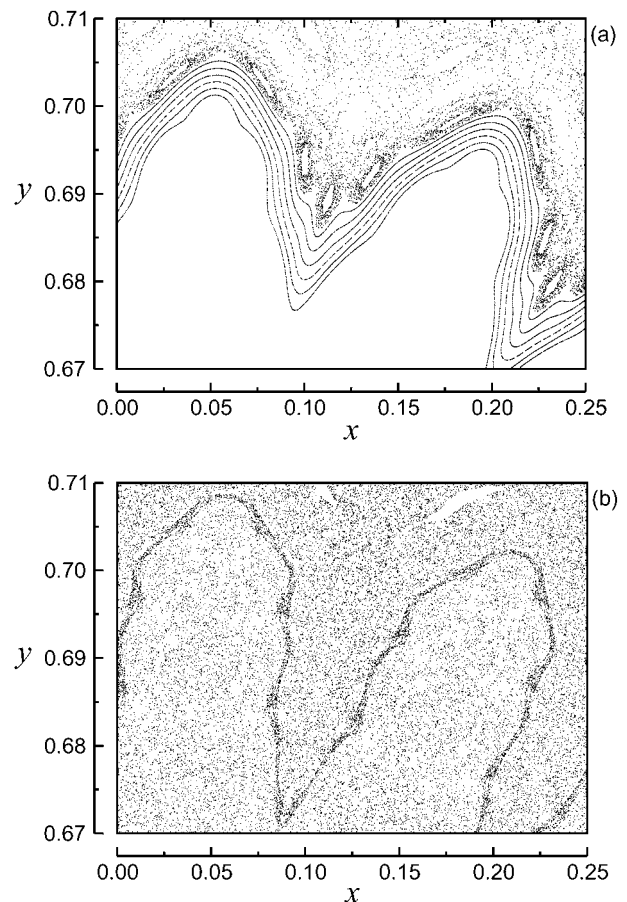

Figure 8. Non-monotonic barrier destruction. Phase portraits show one trajectory above and some on the barrier for different perturbation strengths: (*a*) $I_h/I_p = 0.303$ and (*b*) $I_h/I_p = 0.304$. In the last case the trajectories cross the barrier.

separatrices of islands in this region. This barrier can help plasma confinement preventing energetic charged particles from escaping out radially to an eventual collision with the tokamak inner wall.

Acknowledgments

References

[1] Karger F. and Lackner K. 1977 *Phys. Lett.* A **61** 385
[2] McCool S.C. *et al* 1989 *Nucl. Fusion* **29** 547
[3] Portela J.S.E., Viana R.L. and Caldas I.L. 2003 *Physica* A **317** 411
[4] Heller M.V.A.P. *et al* 2005 *Czech. J. Phys.* **55** 265
[5] Vallet J.C. *et al* 1991 *Phys. Rev. Lett.* **67** 2662
[6] Jakubowski M.W., Abdullaev S.S. and Finken K.H. 2004 *Nucl. Fusion* **44** S1
[7] Mazzucato E. *et al* 1996 *Phys. Rev. Lett.* **77** 3145
[8] Levinton F.M. *et al* 1995 *Phys. Rev. Lett.* **75** 4417
[9] Strait E.J. *et al* 1995 *Phys. Rev. Lett.* **75** 4421
[10] Morrison P.J. 1998 *Rev. Mod. Phys.* **70** 467
[11] Balescu R. 1998 *Phys. Rev.* E **58** 3781
[12] Castillo-Negrete D., Greene J.M. and Morrison P.J. 1996 *Physica* D **91** 1
[13] Petrisor E, Misguich J H and Constantinescu D 2003 *Chaos, Solitons Fractals* **18** 1085
[14] Davidson M.G., Dewar R.L., Gardner H.J. and Howord J. 1995 *Aust. J. Phys.* **48** 871
[15] Howard J E and Hohs S M 1984 *Phys. Rev.* A **29** 418
[16] Corso G, Oda G A and Caldas I L 1997 *Chaos, Solitons Fractals* **8** 1891
[17] da Silva E.C., Roberto M., Caldas I.L. and Viana R.L. 2006 Effects of the resonant modes on the magnetic footprint patterns in a tokamak wall *Phys. Plasmas* **13** at press
[18] Evans T E *et al* 2005 *J. Phys.: Conf. Ser.* **7** 172
[19] da Silva E.C., Caldas I.L. and Viana R.L. 2002 *Phys. Plasmas* **9** 4917
[20] Portela J.S.E., Caldas I.L., Viana R.L. and Sanjuán 2006 Diffusive transport through a nontwist barrier in tokamaks *Int. J. Bifurcat. Chaos* submitted
[21] Wingen A., Spatschek K.H. and Abdullaev S.S. 2005 On the topology of partially stochastic magnetic fields *Workshop on Stochasticity in Fusion Plasmas (Jülich, Germany)* oral presentation
[22] Kucinski M.Y., Caldas I.L., Monteiro L.H.A. and Okano V. 1990 *J. Plasma Phys.* **14** 303
[23] Morse P.M. and Feshbach H. 1953 *Methods of Theoretical Physics* 2nd edn (New York: McGraw-Hill)
[24] da Silva E.C., Viana R.L. and Caldas I.L. 2001 *IEEE Trans. Plasma Sci.* **29** 617
[25] Oda G.A. and Caldas I.L. 1995 *Chaos, Solitons Fractals* **5** 15
[26] Wesson J. 1987 *Tokamaks* (Oxford: Oxford University Press)
[27] Caldas I.L. *et al* 2002 *Braz. J. Phys.* **32** 980
[28] Caldas I.L., Pereira J.M., Ullmann K. and Viana R.L. 1996 *Chaos, Solitons Fractals* **7** 991
[29] Abdullaev S.S. 1999 *J. Phys.* A **32** 2745
[30] Abdullaev S.S. 2002 *J. Phys.* A **35** 2811
[31] Abdullaev S.S. 2004 *Nucl. Fusion* **44** S12
[32] da Silva E.C., Caldas I.L. and Viana R.L. 2002 *Chaos, Solitons Fractals* **14** 403
[33] Lichtenberg A.J. and Lieberman M.A. 1992 *Regular and Chaotic Dynamics* 2nd edn (New York: Springer)
[34] Schaffer M. *et al* 2005 Preliminary study of ITER correction coils for ELM suppression *Workshop on Stochasticity in Fusion Plasmas (Jülich, Germany)* oral presentation
[35] Martin T.J. and Taylor J.B. 1984 *Plasma Phys. Control Fusion* **26** 321
[36] Morrison P.J. 2000 *Phys. Plasmas* **7** 2279
[37] Ullmann K. and Caldas I.L. 2000 *Chaos, Solitons Fractals* **11** 2129